Journal of the Serbian Chemical Society
JSCS@tmf.bg.ac.yu • www.shd.org.yu/JSCS

J. Serb. Chem. Soc. 73 (3) 351–367 (2008)

UDC 621.315.59.004.12:541.135.5–
–0.34.293:546.33–36+544.3

JSCS–3717

Original scientific paper

Semiconducting properties of oxide films formed onto an Nb electrode in NaOH solutions

VLADIMIR D. JOVIĆ*# and BORKA M. JOVIĆ#

Institute for Multidisciplinary Research, 11030 Belgrade, P. O. Box 33, Serbia

(Received 26 June, revised 27 August 2007)

Abstract: In this paper, the results of the potentiostatic formation of homogeneous and heterogeneous, nano-crystalline passive films of Nb_2O_5 onto an Nb electrode in NaOH solutions of different concentrations at potentials lower than 3.0 V *vs.* SCE are presented. The semiconducting properties of such films were investigated by EIS measurements. After fitting the EIS results by appropriate equivalent circuits, the space charge capacitance (C_{sc}) and space charge resistance (R_{sc}) of these films were determined. The donor density (N_{sc}), flat band potential (E_{fb}) and thickness of the space charge layer (d_{sc}) for such oxide films were determined from the corresponding Mott–Schottky (M–S) plots. It is shown that all oxide films were n-type semiconductors in a certain potential range.

Keywords: nano-crystalline; Nb_2O_5; passive film; Mott–Schottky plot; n-type semiconductor.

INTRODUCTION

Among transition metal oxides representing materials having interesting properties, such as superconductivity, colossal magneto-resistance and piezoelectricity, niobium oxides are one of the most interesting. For instance, Nb_2O_5 possesses outstanding dielectric properties, NbO_2 is a semiconductor, while NbO is a metallic conducting material.[1] Due to such properties, they are of high interest for application as devices, optical coatings,[2] solar control and electrochromic films,[3,4] oxygen sensors[5] and capacitors.[6–8] Therefore, procedures for their preparation and evaluation of their properties have attracted considerable attention in recent years. Most of the available data from the materials science approach consider the synthesis of Nb_2O_5 thin films.[9–11]

On the other hand, considerable amount of literature data are available in the field of electrochemical formation, stability and properties of Nb_2O_5 passive films on an Nb electrode in different electrolytes.[12–43] It was shown that a thin passive film, originally formed on an Nb electrode in air, can easily be thickened

* Corresponding author. E-mail: vladajovic@ibiss.bg.ac.yu
# Serbian Chemical Society member.

doi: 10.2298/JSC0803351J

by anodization,[12–16] whereby this process occurs by high-field, ionic migration in the thin film,[12–15] either by metal ions outwards or oxygen ions inwards.[16] It was also shown that the passive oxide film formed on the Nb electrode consists mainly of amorphous Nb_2O_5.[12–14] Its density was determined[17,18] to be 4.74 g cm^{-3}, while its dielectric constant[12] was estimated to be about 45 and that such a film possessed a rather high donor density of the order of 10^{19} cm^{-3} (recently it was found that its value should be 41).[7,8] The value of donor density was ascribed to oxygen vacancies making such a passive oxide film an n-type semiconductor.[19,20] As shown in the book of R. Morrison,[20] an n-type Nb_2O_5 passive film is characterized by a band-gap of 3.4 eV and by a flat band potential of −0.75 V *vs.* SHE at pH 13.0.[22] Some studies have been devoted to the kinetics of the dissolution of naturally formed oxide films[24,25] and to the kinetics of the formation of passive oxide film.[23,26–31] In some cases, EIS[27,32,33] and photoelectrochemical[34] measurements were performed in order to analyze the properties of Nb_2O_5 passive films. An ellipsometric study revealed that with increasing anodic potential in the range from 2.0 to 10.0 V *vs.* SHE in 1.0 M H_2SO_4, the thickness of the Nb_2O_5 film increased linearly from about 10 nm to about 28 nm,[28] with the simultaneous evolution of oxygen at potentials higher than 2.0 V *vs.* SHE. Most recently it was shown that by combination of anodization – annealing – anodization techniques, porous Nb_2O_5 films of thickness of more than half a micrometer could be formed onto an Nb electrode in 1.0 M H_3PO_4 with the addition of 1.0 wt. % HF at 5.0 °C at 2.5 V *vs.* Ag|AgCl (3.0 M KCl) followed by annealing under a nitrogen atmosphere at different temperatures for 3 h.[35] It is important to note that the electrochemical behavior of Nb (corrosion and passive oxide film formation) were mainly investigated in a relatively narrow potential range, from about –1.3 to about 1.0 V *vs.* SCE,[23–31] while the properties of Nb_2O_5 passive films were mainly investigated for the films obtained under high-voltage anodized Nb.[12–20,27,33,34] The semiconducting properties of passive oxide films formed at potentials lower than 2.0 V *vs.* SCE have practically not been reported in the literature hitherto.

In this study an attempt was made to grow potentiostatically Nb_2O_5 passive films in NaOH electrolyte of different concentrations at potentials lower than 3.0 V *vs.* SCE and to investigate their semiconducting properties by analysis of EIS results and M–S plots.

EXPERIMENTAL

All experiments were carried out in a three-compartment standard electrochemical cell at room temperature in an atmosphere of purified nitrogen. Before each experiment, the electrolyte was purged with N_2 for 30 min. The same N_2 atmosphere was maintained over the solution during the experiment to minimize oxygen contamination. A platinum mesh counter electrode and the reference, saturated calomel electrode (SCE), were placed in separate compartments. The latter was connected to the working electrode by a Luggin capillary. All solutions were made from analytical grade NaOH (Merck) and extra pure UV water (Smart2PureUV, TKA).

Polarization, chronoamperometric and EIS measurements were performed by a computer-controlled Gamry potentiostat (Reference 600) using Corrosion Software DC 105, Physical Electrochemistry Software PHE 200 and Electrochemical Impedance Software EIS 300.

Contact of the Nb (99.9% Goodfellow) sample ($1.0\times1.0\times0.2$ cm^3) with a copper wire on the back side of the electrode was made with silver conductive epoxy paste (Alfa Aesar) and electrode was sealed in an epoxy resin so that only an area of 1.0 cm^2 was exposed to the solution. Once mounted, the electrode was polished first on emery papers (1200, 2400 and 4000) and then on polishing clothes impregnated with alumina down to 0.05 μm (1, 0.3 and 0.05 μm), cleaned in an ultrasonic bath for 10 min (to remove traces of polishing alumina), thoroughly washed with extra pure UV water and transferred to the electrochemical cell in which the chronoamperometric, polarization and EIS measurements were performed.

Before the polarization measurements, the Nb electrode was kept at the open circuit potential for 10 s and cathodic limit was set at −1.35 V. The polarization diagrams were recorded at a sweep rate of 1.0 mV s^{-1} starting from the cathodic limit and finishing at 3.0 V in 0.25 M NaOH and at 2.0 V in 2.50 M and 5.00 M NaOH. The formation of passive oxide films was performed by the following procedures: in 0.25 M NaOH, the potential was first set at 1.0 V for 1 h and then at 3.0 V for 2 h; in 2.50 M NaOH, the potential was first set at 1.0 V for 1 h and then at 2.0 V for either 3 h or 6 h; in 5.00 M NaOH, the potential was first set at 1.0 V for 1 h and then at 2.0 V for 1 h. The corresponding current density *vs.* time responses were also recorded. After passive oxide film formation, EIS spectra were recorded at different potentials, covering the potential region B (see Fig. 1), starting from the most positive one (usually 2.0 V, except for 0.25 M NaOH where the starting potential was 2.7 V) down to a potential of 0.5 or 0.6 V. All EIS spectra were recorded in the 0.1 Hz to 40 kHz frequency range with ac amplitude of 10 mV. After completion of these measurements, EIS spectra for certain potentials in the range 0.6–2.0 V (for example 1.0 V, 1.5 V and 2.0 V) were recorded again to determine whether the property of the passive film had changed during this procedure. It was found that the maximum difference between the first and repeated experiments was in the range of ±5 %, confirming that the properties of the passive film remained the same during the impedance measurements.

Scanning electron microscopy was performed using a VEGA TS 5130 MM (TESCAN) microscope.

RESULTS

The polarization diagrams recorded in three concentrations of NaOH (marked in the Figure) are shown in Fig. 1. As can be seen, all the diagrams are characterized by a corrosion potential (being more negative at higher concentrations of NaOH) followed by a sharp increase and a peak of the current density. This peak is seen to be more pronounced at higher concentrations of NaOH. At more positive potentials (region B on the diagram), all polarization curves are characterized by a current density plateau up to the potential of region C (dashed line in Fig. 1). In the potential region C, a second current density increase is seen to occur in all solutions, followed again by a current density plateau up to the upper applied potential limit (2.0 or 3.0 V).

The current density *vs.* time responses (*j vs. t*) for the formation of passive films in 0.25, 2.50 and 5.00 M NaOH are presented in Fig. 2a, 2b and 2c, respectively. The first applied potential of 1.0 V was approximately the potential of

the second peak (second current density increase) in all solutions, while the second applied potential was the maximum potential recorded on the polarization diagrams (Fig. 1). As can be seen, the *j vs. t* transients recorded in 0.25 and 2.50 M NaOH solutions were monotonously falling transients for both applied potentials, while in the case of 5.00 M NaOH, first transient (1.0 V) was characterized by a current density increase after about 1000 s.

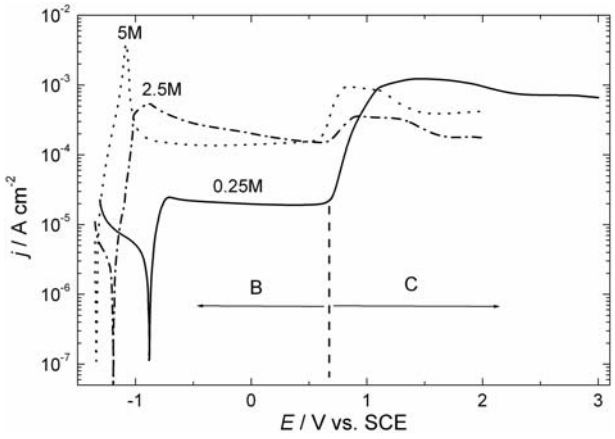

Fig. 1. Polarization diagrams recorded onto Nb electrode at a sweep rate of 1.0 mV s^{-1} in NaOH solutions of different concentrations (marked in the Figure).

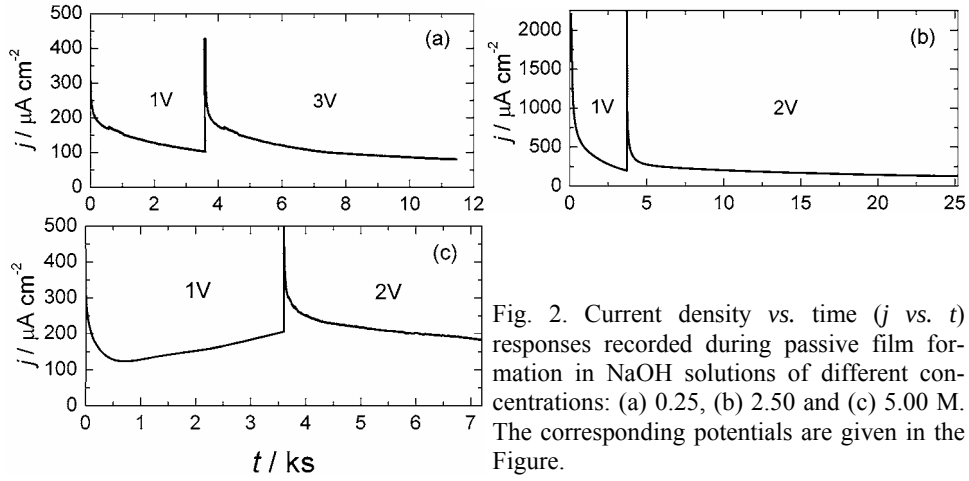

Fig. 2. Current density *vs.* time (*j vs. t*) responses recorded during passive film formation in NaOH solutions of different concentrations: (a) 0.25, (b) 2.50 and (c) 5.00 M. The corresponding potentials are given in the Figure.

The equivalent circuits used for fitting the EIS results are presented in Fig. 3. In all cases for 0.25 and 2.50 M NaOH, the best fit was obtained with the equivalent circuit (a). For the highest NaOH concentration of 5.00 M, the EIS results were of a different shape, characteristic for the surface charge approach[35–37] and these results were fitted with the equivalent circuit (b), used in the literature for such an approach.[31,33,35–37] The parameters of the corresponding equivalent circuits are: (a) R_s – solution resistance; CPE_{sc} – constant phase element corres-

ponding to the space charge capacitance[38] ($Z_{CPE} = Y_0(j\omega)^{\alpha}$); R_{sc} – space charge resistance; (b) R_s – solution resistance; C_0 – Faradaic pseudocapacitance; C_b – barrier film capacitance; R_b – resistance of defect migration; R_{SC} and L_{SC} – elements associated with the negative surface charge at the film/solution interface.[31,33,35–37]

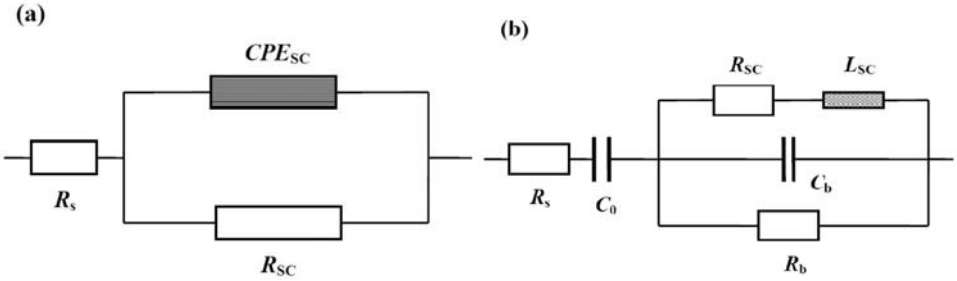

Fig. 3. Equivalent circuits used for fitting the EIS results.

Typical experimental EIS results (squares, circles, triangles, *etc*.) together with the fitting curves (solid lines) obtained in 0.25 and 2.50 M solutions are presented in Fig. 4. Actually, Fig. 4 represents the results obtained with the passive oxide film formed for 1 h at 1.0 V and for 3 h at 2.0 V in 2.50 M NaOH. The *Z*'–*Z*'' diagrams recorded at each potential are presented in Fig. 4 and the corresponding potentials are marked in V (a – potentials from 2.0 to 1.3 V and b – potentials from 1.2 to 0.6 V). In general, the shape of all diagrams recorded in 0.25 and 2.50 M NaOH were identical to those in Fig. 4, except that the values of *Z*' and *Z*'' were different for different cases. A characteristic of the fitting results for these *Z*'–*Z*'' diagrams is that the heterogeneity factor in the *CPE*s (α) is, in all cases, very close to unity (varying between 0.95 and 0.98), indicating that the space charge of the oxide films was almost homogeneously distributed in the film (see Discussion).

The EIS results obtained for the oxide film formed in 5.00 M NaOH are shown in Fig. 5 (the squares, circles, triangles, *etc*. are experimental points, the solid lines are the fitting results). The shape of the *Z*'–*Z*'' diagrams is characteristic for the surface charge approach and, accordingly, the experimental results were fitted with the equivalent circuit developed for such an approach, presented in Fig. 3b. All the *Z*'–*Z*'' diagrams were recorded in the range from 2.0 to 0.8 V and the low frequency limit was set at 0.50 Hz (some of the diagrams are shown in Fig. 5a). One *Z*'–*Z*'' diagram, recorded for a potential of 1.4 V, was repeated (after the whole set of experiments were finished) with the low frequency limit set at 0.10 Hz. This diagram is presented in Fig. 5b. The experimental results in Fig. 5 were fitted by the equivalent circuit presented in Fig. 3b (dotted line) and by the same equivalent circuit where C_0 was replaced by *CPE* (solid line). As can be seen, a much better fit was obtained with *CPE*. Hence, all the experimental

results were fitted by both equivalent circuits and the small difference was recorded for the parameters plotted in Fig. 7a and 7b. On the other hand, the values of C_0 varied between 2259 and 3761 μF cm^{-2}, most likely indicating a high roughness of the electrode surface and the possible adsorption of anions onto the passive film. At the same time, when fitting the EIS results with *CPE* instead of C_0, the heterogeneity factor in the *CPE*s (α) was found to vary between 0.613 and 0.762, also indicating a heterogeneous distribution of charge at the oxide/electrolyte interface.

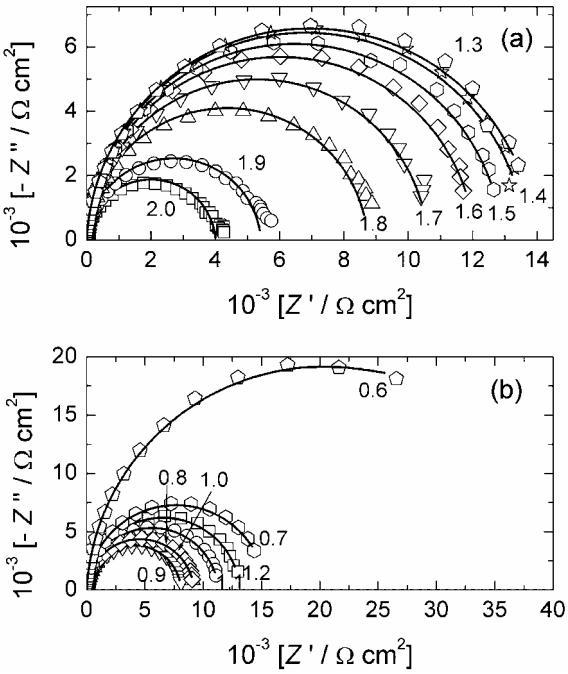

Fig. 4. *Z*'–*Z*'' Diagrams recorded in 2.50 M NaOH after passive film formation for 1 h at 1.0 V and 3 h at 2.0 V. The corresponding potentials are marked in V: (a) from 2.0 to 1.3 V; (b) from 1.2 to 0.6 V. The experimental points are presented by squares, circles, triangles *etc*., while the solid lines represent the fitted curves obtained using the equivalent circuit presented in Fig. 3(a). Frequency range: from 40 kHz to 0.10 Hz.

The M–S plots shown in Fig. 6 were obtained by analysis of the EIS results for: (a) 0.25, (b) 2.50 and (c) 5.00 M NaOH. As can be seen in Fig. 6a, linear M–S plot were obtained for the concentration of 0.25 M in the potential range from 2.5 to 1.4 V, while in the case of 2.50 and 5.00 M NaOH, well defined M–S plots were obtained over the whole investigated range of potentials for both passive films. These results indicate that n-type semiconducting oxide films are formed in all cases.

The results presented in Fig. 7 were obtained by analysis of the *Z*'–*Z*'' diagrams shown in Fig. 5. The squares represent the results obtained by fitting the *Z*'–*Z*'' diagrams using the equivalent circuit presented in Fig. 3b, while the circles represent the results obtained by the fitting *Z*'–*Z*'' diagrams using the same equivalent circuit with C_0 being replaced by *CPE*. As can be seen in Fig. 7a and 7b, linear dependences (predicted by the model) were obtained for C_b^{-1} *vs.* *E*

and $R_b j$ *vs.* E. The steady-state current density used to plot $R_b j$ *vs.* E is the current density recorded at the end of the pulse presented in Fig. 2c. To obtain all the model parameters (see discussion), the (R_b/R_{sc}) *vs.* E and ($L_{sc} j /R_{sc}$) *vs.* E dependences are plotted in Fig. 7c and 7d, respectively, for all the investigated potentials. Although the model of surface charge approach does not consider a linear dependence for C_b^{-2} *vs.* E (M–S plot), this dependence was also recorded, as shown in Fig. 6c.

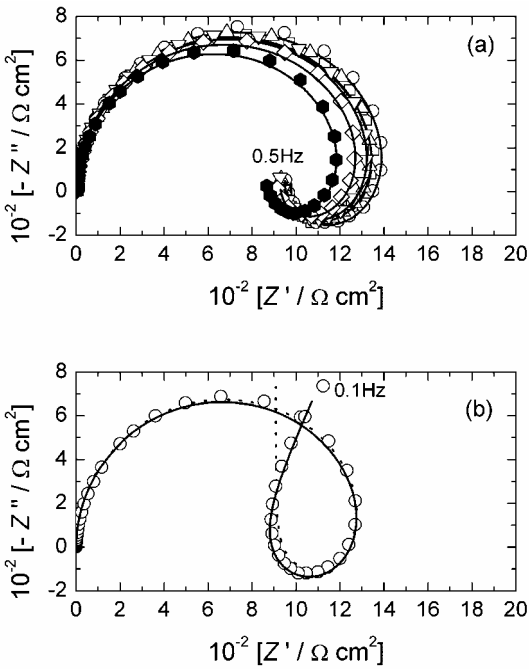

Fig. 5. (a) Z'–Z'' Diagrams recorded in 5.00 M NaOH after passive film formation for 1 h at 1.0 V and 1 h at 2.0 V. The corresponding potentials: □ 1.9, ○ 1.7, △ 1.5, ▽ 1.3, ◇ 1.1 and ⬢ 0.9 V. The experimental points are presented by squares, circles, triangles *etc.*, while the solid lines represent the fitted curves obtained using the equivalent circuit presented in Fig. 3(b). Frequency range: from 40 kHz to 0.50 Hz. (b) Z'–Z'' Diagram in the same solution under the same conditions of passive film formation: potential 1.4 V. The experimental points are presented by circles. The dotted line represents the fitted curve obtained using the equivalent circuit presented in Fig. 3(b), while the solid line represents the fitted curve obtained using the same equivalent circuit but with C_0 being replaced by *CPE*. Frequency range from 40 kHz to 0.10 Hz.

The SEM micrographs of the surface of the oxide films formed in 2.50 M NaOH by the pulse procedure (b), Fig. 2, and in 5.00 M NaOH by the pulse procedure (c), Fig. 2, are presented in Fig. 8a and 8b, respectively.

The M–S plots obtained by analysis of the EIS results recorded in 2.50 M NaOH are presented in Fig. 9a and 9b, assuming that the impedance of the process occurring in the semiconducting oxide film could be presented by the parallel connection of C_{sc} and R_{sc} or the serial connection of C_{sc} and R_s, respectively (see Discussion).

The properties of the space charge layer (slopes of the M–S plots, donor densities, N_{sc}, flat band potentials, E_{fb}, and thicknesses of the space charge layer, d_{sc}), obtained by the analysis of M–S plots presented in Fig. 6, as a function of the NaOH concentration and the conditions of the formation of Nb_2O_5 film are presented in Table I.

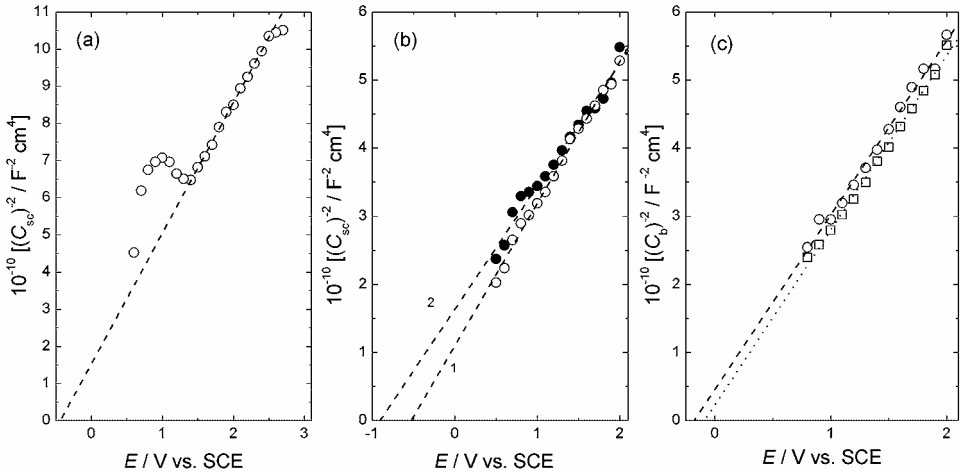

Fig. 6. M–S plots for the passive films formed in: (a) 0.25, (b) 2.50 (1 – 1 h at 1.0 V followed by 3 h at 2.0 V; 2 – 1 h at 1.0 V followed by 6 h at 2.0 V) and (c) in 5.00 M NaOH (□ − C_b values obtained by fitting the EIS results using the equivalent circuit presented in Fig. 3(b); ○ − C_b values obtained by fitting the EIS results using the same equivalent circuit but with C_0 being replaced by *CPE*).

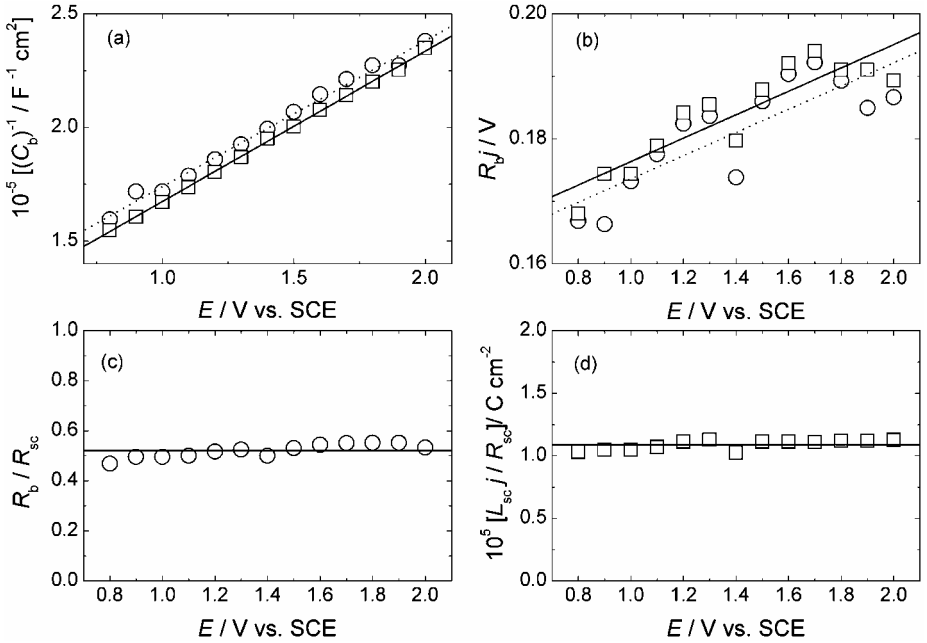

Fig. 7. (a) C_b^{-1} *vs. E*, (b) $R_b j$ *vs. E*, (c) (R_b/R_{sc}) *vs. E* and (d) ($L_{sc} j /R_{sc}$) *vs. E* dependences obtained by fitting the EIS results presented in Fig. 5. (□) C_b, R_b, R_{sc} and L_{sc} values obtained by fitting the EIS results using the equivalent circuit presented in Fig. 3b; (○) C_b, R_b, R_{sc} and L_{sc} values obtained by fitting the EIS results using the same equivalent circuit but with C_0 being replaced by *CPE*.

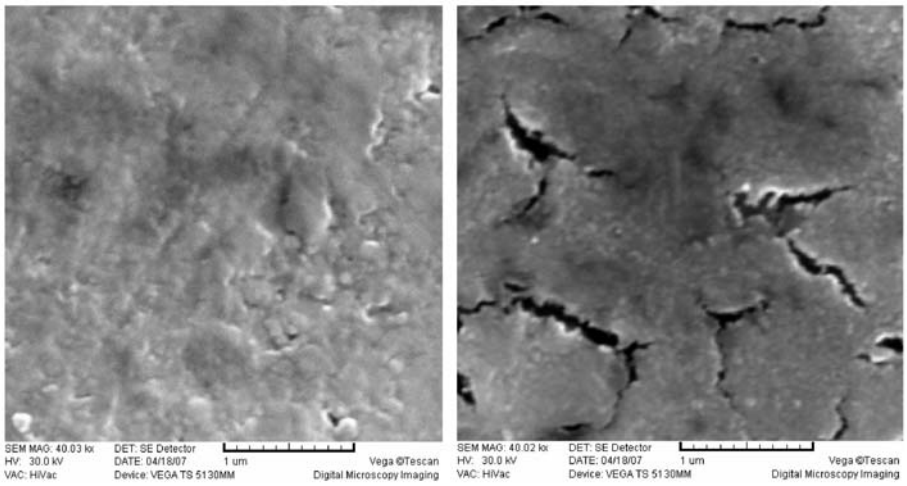

Fig. 8. (a) SEMs of the Nb_2O_5 surface formed in 2.50 M NaOH by pulse procedure (b) in Fig. 2; (b) SEMs of the Nb_2O_5 surface formed in 5.00 M NaOH by pulse procedure (c) in Fig. 2.

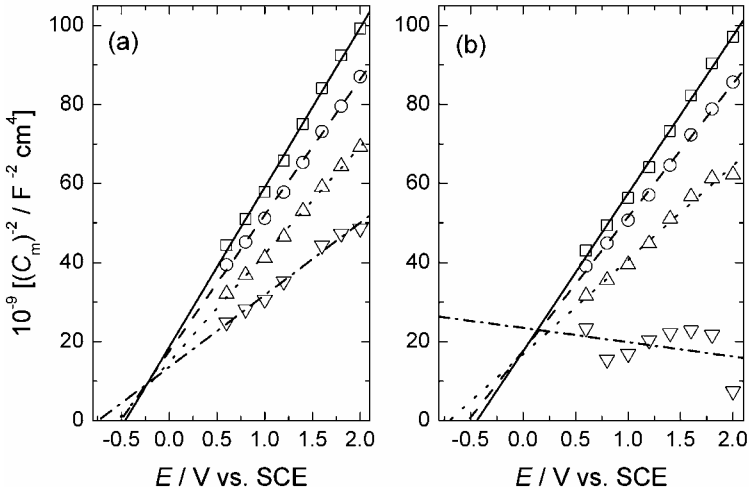

Fig. 9. M–S plots calculated from the EIS data recorded in 2.50 M NaOH for the film formed with 1 h at 1.0 V and 3 h at 2.0 V, assuming (a) parallel connection of C_{sc} and R_{sc} and (b) serial connection of C_{sc} and R_{sc} for different frequencies: □ − 10 kHz; ○ − 1 kHz; △− 100 Hz and ▽− 10 Hz.

DISCUSSION

Polarization diagrams

According to the available literature, the formation of a passive film on Nb is very sensitive to the pre-treatment of the electrode.[30] In order to avoid the for-

mation of Nb hydrides[40,41] of a wide non-stoichiometric composition[42] which are usually formed at about −1.5 V *vs.* SHE,[30] all polarization diagrams were recorded starting from the same cathodic potential limit of −1.35 V *vs.* SCE, *i.e.*, about −1.0 V *vs.* SHE (after 10 s at the open circuit potential). As can be seen in Fig. 1, with increasing NaOH concentration, the corrosion potential becomes more negative, which is in accordance with previous investigations.[26] Simultaneously, the peak of Nb dissolution and Nb_2O_5 oxide formation,[26] appearing at slightly more positive potentials than the corrosion potential, was found to increase with increasing NaOH concentration. At more positive potentials than the peak potential, the sudden decrease in the current density indicates a well-defined passive behavior of Nb (Nb_2O_5 passive film) and this is characteristic for the potential region marked B in Fig. 1. With further increase of the potential in all three solution concentrations, a further increase in current density could be detected, indicating that a new process occurs at the passive Nb_2O_5 film. Such a behavior was detected in a few previously published papers,[30,32,34] but none of the authors attempted to explain it. Characteristic for the potential region C is that after the increase in current density a more or less well defined current density plateau could be detected in all the investigated solutions, with the one in 0.25 M NaOH being the best defined. Since a break-down of passive Nb_2O_5 film was found not to occur to 10 V[30] and even up to 80 V,[6] this current density increase could be ascribed to either further oxidation of the passive Nb_2O_5 layer or some other process, such as the accumulation of oxygen vacancies in the oxide film, since it was shown that oxygen vacancies are donors in such an n-type semiconducting film.[19,20] It is most likely that this process represents the accumulation of oxygen vacancies in the oxide film, since all three oxides of Nb should be formed at negative potentials (NbO at −1.57, NbO_2 at −1.46 and Nb_2O_5 at −1.128 V *vs.* SHE[43]) and, simultaneously, the only oxide detected by the X-ray diffraction technique[32] at potentials more positive than 2.0 V *vs.* SCE was Nb_2O_5.

Passive oxide film formation at constant potentials

As can be seen in Fig. 2, in all cases, passive oxide films were formed by applying two potentials: first at 1.0 V (approximately the potential of the current density maximum in the potential region C) for 1 h and then at the potential of the upper limit on the polarization curves for different time durations (2, 3, 6, and 1 h). Such a procedure was employed in order to obtain an as homogeneous as possible oxide film and it is obvious that this was achieved since the factor of the space charge layer homogeneity α was very close to 1 (see results). Also, with such a procedure of passive oxide film formation the possibility for Nb hydride formation[30] was avoided. It is characteristic for Fig. 2 that only in 5.00 M NaOH did the current density commence to increase after about 1000 s at the potential of 1.0 V, indicating a possible increase of the surface area, most likely by an increase of the roughness of the electrode surface, which was confirmed by the

values for the Faradaic pseudocapacitance values (C_0), which varied between 2259 and 3761 μF cm^{-2} for such a passive oxide film (Fig. 5 – see discussion of the EIS results) and by the SEM presented in Fig. 8b, with the passive oxide film surface being characterized by the presence of a significant number of open pores (cracks) of length about 0.5 μm and width about 0.1 μm. As can be seen in Fig. 8a, the surface of the passive oxide film formed in 2.50 M NaOH (pulse procedure (b) – Fig. 2) was homogeneous, while the one formed in 5.00 M NaOH (pulse procedure (c) – Fig. 2) was heterogeneous. The crystals of both films are extremely small, being of the order of about 20 nm maximum (this could be estimated at higher magnification, but the picture was not very clear and is not presented here).

EIS Results analysis

As can be seen in Fig. 4, all the EIS spectra recorded in 0.25 and 2.50 M NaOH solutions in the frequency range 0.10–40 kHz were characterized by well defined semi-circles on the Z'–Z'' diagrams. After fitting them with the equivalent circuit presented in Fig. 3a, very good fits were obtained, indicating that in the given frequency range, a double layer capacitance could be neglected and that the whole process is dominated by a space charge capacitance and a resistance. In order to obtain the dimensionally correct value for the space charge capacitance (C_{sc}), the following Equation was used:[44]

$$C_{sc} = (Y_0 R_{sc}^{1-\alpha})^{\frac{1}{\alpha}} \quad (1)$$

which is derived from the Equation:[45]

$$C_{sc} = Y_0(\omega''_m)^{\alpha-1} \quad (2)$$

where Y_0 represents the constant in the equation for the constant phase element[39] in all commercially available software (given in Ω^{-1} cm^{-2} s$^{\alpha}$), ω''_m is the frequency of the maximum on the $-Z''$ *vs.* log ω dependence (independent of the value of α) and α is the factor of the charge distribution homogeneity in the passive oxide film. It is important to note that in such approach it is assumed that both components of the space charge layer (C_{sc} and R_{sc}) are dependent on α (these equations are generally developed for parallel connection of *CPE* and R[44–46]). After the fitting procedure and calculation of C_{sc}, these values were used to plot the dependences shown in Fig. 6. From the slopes of the M–S plots, the values of the donor densities (N_{sc}) were calculated using the dielectric constant for Nb_2O_5, $\varepsilon = 41$.[7] These values are given in Table I for all the passive oxide films together with the values of the flat band potential (E_{fb}), obtained from the intercept at the potential axis. As can be seen, the lowest value of N_{sc} was obtained for the oxide film formed in 0.25 M NaOH, while the highest value was obtained for the film formed in 2.50 M NaOH with the duration of the second pulse at 2.0 V being 6 h, indicating that the number of donors (in this case oxygen vacancies) increased with the time of electrode polarization at a given anodic potential. Also, it should

be noted that the increase of N_{sc} was accompanied by a more negative value of E_{fb}, which is in accordance with the theory of semiconducting processes[19,20] (an increase in N_{sc} lowers the slope of the M–S plot and accordingly the intercept at the potential axis is shifted to more negative potentials).

TABLE 1. Conditions of Nb_2O_5 film formation and oxide semiconducting properties

NaOH Conc.	Condition of oxide film formation	Slope of M–S plot F^{-2} m^4 V^{-1}	$N_{sc}\times10^{-20}$ cm^{-3}	E_{fb} V *vs.* SCE	d_{sc} nm
0.25 M	1 h at 1.0V + 2 h at 3.0V	351	0.98	–0.44	12.56
2.50 M	1 h at 1.0V + 3 h at 2.0V	208	1.65	–0.54	8.30
2.50 M	1 h at 1.0V + 6 h at 2.0V	180	1.91	–0.92	8.28
5.00 M	1 h at 1.0V + 1 h at 2.0V	256	1.34	–0.19	8.54

The thickness of the space charge layer, d_{sc}, was calculated using the Equation:[47,48]

$$d_{sc} = \left[\frac{2\varepsilon\varepsilon_0}{eN_{sc}} (E - E_{fb} - \frac{kT}{e}) \right]^{1/2} \quad (3)$$

where ε_0 represents the permittivity of free space, E is the potential of the passive oxide film formation (the value of the second pulse, either 2.0 or 3.0 V), while e, k and T have their usual meanings. As can be seen, the highest value of the space charge layer thickness was obtained at the most positive potential of 3.0 V (in accordance with the literature[6,28]), while with the duration of the second pulse, the thickness of the space charge layer does not change but the donor density increases and the flat band potential becomes more negative (line 2 in Fig. 6b).

In the case of 5.00 M NaOH solution, a completely different shape of Z'–Z'' diagrams, characterized by the presence of an inductive loop, was obtained (Fig. 5). According to Bojinov *et al.*[36–38], such EIS results are typical for the surface charge approach, *i.e.*, film growth is limited by both high-field assisted bulk migration and relaxation of the charge carrier density (in this case oxygen vacancies) at the metal/film interface. During such a process, a thin continuous barrier-like layer of a wide band-gap semiconductor is formed. This theory predicts several linear dependences for the parameters obtained by fitting the EIS results using the equivalent circuit shown in Fig. 3b, two of them being: C_b^{-1} *vs.* E and $R_b j$ *vs.* E. As can be seen in Fig. 7a and 7b, respectively, both of them are linear in the investigated potential range. Simultaneously, as the model predicts (see Eqs. (6) and (7)), the functions (R_b/R_{sc}) *vs.* E and ($L_{sc} j/R_{sc}$) *vs.* E are independent of potential (Fig. 7c and 7d, respectively). For the same system, Nb in 5.00 M NaOH, but at more positive potentials (2.0 V > E > 10.0 V) and a high temperature of 50 °C, similar dependences were obtained.[32]

According to the literature,[32,36–38] the parameters for the surface charge model can be calculated from the following Equations:

$$\frac{\mathrm{d}(R_\mathrm{b} j)}{\mathrm{d}E} = \frac{RT}{zFaE_\mathrm{f}} \tag{4}$$

$$\frac{\mathrm{d}(C_\mathrm{b}^{-1})}{\mathrm{d}E} = \frac{(1-\delta)}{\varepsilon\varepsilon_0 E_\mathrm{f}} \tag{5}$$

$$\frac{R_\mathrm{b}}{R_\mathrm{sc}} = \frac{\delta}{(1-\delta)} \tag{6}$$

$$\frac{L_\mathrm{sc} j}{R_\mathrm{sc}} = S \tag{7}^{38}$$

and

$$\frac{L_\mathrm{sc} j}{R_\mathrm{sc}} = \frac{1}{S} * \tag{7a}^{32}$$

$$C_0 = \frac{nF(1-\delta)}{V_\mathrm{m}\lambda E_\mathrm{f}} \tag{8}$$

where E_f is the electric field in the film bulk; a, the half-jump distance of the oxygen vacancies; S, the capture cross-section for positive defects by the negative surface charge; δ, the polarizability of the film/solution interface; λ, the current efficiency for film formation under transient conditions; V_m, the molar volume of the oxide; n, the number of elementary changes necessary to grow an oxide (for Nb_2O_5, $n = 10$) and z is the electric charge of the mobile species (in this case $z = 2$, charge transport occurs by oxygen vacancies, since it is assumed that the transport of oxygen vacancies is much faster than that of metal ones). Using the parameters of the surface charge model obtained from above Equations, it is possible to calculate the formation ratio dx/dE, which in this case does not simply coincide with the reciprocal of the electric field (traditional high field model[49]), but, according to Chao *et al.*,[50] is linked to the electric field and the polarizability of the oxide film/solution interface (point defect model) by the Equation:

$$\frac{\mathrm{d}x}{\mathrm{d}E} = \frac{1-\delta}{E_\mathrm{f}} \tag{9}$$

The model parameters obtained using Eqs. (4)–(9) and the results presented in Fig. 7 are: $E_\mathrm{f} = 2.83\times10^6$ V cm^{-1}; $S = 1.1\times10^{-5}$ C cm^{-2} (according to Ref. 38), or $S = 91$ mC^{-1} cm^2 (according to Ref. 32); $\delta = 0.34$; $\lambda_\mathrm{av.} \approx 1$; $a = 4.88$ nm and dx/d$E = 2.33$ nm V^{-1}. Hence, if the results obtained in Ref. 32 are compared with those presented in this paper, it could be concluded that, except for S and λ, the other parameters are in good agreement. It should be emphasized here that λ_av presented in this paper (calculated from Eq. (8)) was obtained as an average value, since the Faradaic pseudocapacitance value (C_0) varied between 2259 and 3761

* It should be noted that in both references[38,32] the value of S is given in C^{-1} cm^2.

μF cm^{-2} in the investigated potential range, with no indication of any linearity, indicating 100 % current efficiency for the formation of the oxide film under the given conditions. It is important to mention here that a significant difference in the surface of the passive oxide films obtained in Ref. 32 and in this paper exists. In Fig. 6 of Ref. 32, well-defined needle-like crystals (several tens of microns long and about 1 μm wide, randomly oriented) were detected on the Nb_2O_5 surface after 60 min of polarization at 4.0 V *vs.* SCE in 5.00 M NaOH at 50 °C, while in the present case, after 1 h at 1.0 V and 1 h at 2.0 V at 25 °C, a heterogeneous (with the presence of cracks – open pores), nano-crystalline Nb_2O_5 surface was obtained. Such a difference in the morphology of the Nb_2O_5 surface is the most likely reason for the difference in the parameters S and λ given in Ref. 32 and in this paper. It is also important to note that a much better fit of the experimental results presented in Fig. 5a would be obtained using *CPE* instead of C_0, which indicates that the calculation of λ would be more accurate after fitting the experimental results with *CPE*. Unfortunately, since there was no parallel resistance in connection with C_0, the use of Eqs. (1) or (2) was not possible and the fitting results could give only a value of Y_0 which could not be used for the calculation of λ since its dimension is given in Ω^{-1} cm^{-2} s^{α}.

It is interesting to note that for the same system, a C_b^{-2} *vs.* E (M–S) dependence, shown in Fig. 7c, was also detected. Since the surface charge model predicts the existence of a thin continuous barrier-like layer of a wide band-gap semiconductor, it seems reasonable to obtain well defined M–S plots.

A simplification of the process occurring at semiconducting electrodes, assuming either a serial connection of C_{sc} and R_s or a parallel connection of C_{sc} and R_{sc}, is very often used in the literature.[24,51–56] At the same time, in most commercially available software for M–S plots, a serial connection is assumed, while in the case of EIS300 software of Gamry both situations can be used. In the case of serial connection of C_{sc} and R_s, the capacitance is calculated directly from the value of Z'', *i.e.*, $C_{sc} = 1/2\pi fZ''$ and plotted as C_m^{-2} *vs.* E, while in the case of parallel connection of C_{sc} and R_{sc}, the capacitance is calculated directly from the value of Y'', *i.e.*, $C_{sc} = Y''/2\pi f$ and plotted as C_m^{-2} *vs.* E. The results of such an approach for different frequencies (□ – 10 kHz; ○ – 1.0 kHz; △ – 100 Hz and ▽ – 10 Hz) are presented in Fig. 9 for the passive Nb_2O_5 film formed in 2.50 M NaOH for 1 h at 1.0 V and 3 h at 2.0 V. As can be seen, in both cases well-defined linear M–S plots were obtained with their slopes changing with the frequency. In case (a), the slope changed in the range of about 421–202 F^{-2} m^4 V^{-1}, with the corresponding N_{sc} values varying in the range 0.82×10^{20}–1.70×10^{20} cm^{-3} (accordingly E_{fb} changed from −0.47 to −0.73 V). Comparing these values with the one presented in Table I for this particular oxide film, it appears that in case (a) a low frequency of 10 Hz should be used in order to obtain agreement with the N_{sc} values determined by fitting the EIS spectra. In case (b), a positive slope was obtained for 10, 1.0 and 0.100 kHz, while for 10 Hz, the slope was negative.

The positive slope changed in the range 399–239 F^{-2} m^4 V^{-1}, with the corresponding N_{sc} values varying in the range 0.86×10^{20}–1.44×10^{20} cm^{-3} (accordingly E_{fb} changed from −0.44 to −0.72 V). Hence, in case (b), the M–S plot for 0.100 kHz should be used in order to obtain agreement with the N_{sc} values determined by fitting the EIS spectra. It is most likely that the change of the slope of the M–S plots is a consequence of the fact that the capacitance is not an exactly parallel plate condenser but is represented by the *CPE* and, although the values of α are close to unity (0.95–0.98), the values of C_{sc} are sensitive to such small deviations from unity. It is also important to note that in case (b), at a frequency of 10 Hz ($\triangledown$), such an approach is not recommended, since the slope of the corresponding M–S plot changes, leading to the eventual conclusion that the investigated oxide film is a p-type semiconductor. Usually such an approach is used in the literature[24,51–56] at only one constant frequency (1.0 kHz in most cases), assuming that at such a particular frequency, the system could be described by the serial connection of the solution resistance and the oxide film capacitance (neglecting the contribution of the double layer capacitance). This is a correct assumption but, on the other hand, for impedance spectra of almost all systems this assumption (simplification) is valid. Hence, it seems reasonable to avoid direct M–S plots and obtain correct values of C_{sc} by fitting the EIS results and then plotting the corresponding M–S plots.

CONCLUSIONS

According to the results presented in this paper, homogeneous, nano-crystalline passive films of Nb_2O_5 could be formed onto an Nb electrode by a proper potentiostatic pulse procedure at potentials more negative than 3.0 V *vs.* SCE at concentrations of NaOH equal to, or lower than, 2.50 M. It was shown that such films are n-type semiconductors. Their semiconducting properties were found to be different depending on the conditions of the film formation (NaOH concentration and pulse regime). In 5.00 M NaOH, the properties of the passive film could be explained by the surface charge model, with the passive oxide film being heterogeneous.

И З В О Д

ПОЛУПРОВОДНИЧКА СВОЈСТВА ОКСИДНИХ ФИЛМОВА ФОРМИРАНИХ НА Nb ЕЛЕКТРОДИ У РАСТВОРУ NaOH

ВЛАДИМИР Д. ЈОВИЋ И БОРКА М. ЈОВИЋ

Институт за мултидисциплинарна истраживања, п. пр. 33, 11030 Београд

У овом раду приказани су резултати потенциостатског формирања хомогених и хетерогених, нано-кристалних, пасивних филмова Nb_2O_5 на електроди од ниобијума у растворима NaOH различитих концентрација и на потенцијалима мањим од 3,0 V према ЗКЕ. Полупроводничка својства оваквих филмова испитивана су EIS методом. Након фитовања EIS резултата одговарајућим еквивалентним колом одређиване су вредности “space charge” капацитета (C_{sc}) и “space charge” отпора (R_{sc}). Густина носилаца наелектрисања (N_{sc}), “flat band”

потенцијал (E_{fb}) и дебљина "space charge" слоја (d_{sc}) ових оксидних филмова одређена су из одговарајућих Mott–Schottky зависности. Показано је да се у 5,00 M NaOH формира хетерогени оксидни филм са отвореним порама (пукотинама) на површини, док се при нижим концентрацијама NaOH формира компактан и хомоген оксидни филм. Mott–Schottky зависности са позитивним нагибом, регистроване за све добијене филмове, потврђују да су из свих раствора добијени полупроводнички филмови n–типа.

(Примљено 26. јуна, ревидирано 27. августа 2007)

REFERENCES

1. Y. Zhao, Z. Zhang, Y. Lin, *J. Phys. D: Appl. Phys.* **37** (2004) 3392
2. J. J. van Gladbeek, R. E. van De Leest, *Thin Solid Films* **201** (1991) 137
3. N. Ozer, M. D. Rubin, C. M. Lampert, *Sol. Energy Mater. Sol. Cells* **40** (1996) 285
4. C. G. Granquist, *Solid State Ion.* **53** (1992) 479
5. D. Rosenfeld, R. Sanjines, F. Levy, P. A. Buffat, V. Demame, A. Gisel, *J. Vac. Sci. Technol.* **A12** (1994) 135
6. http://www.lem.uni-karlsruhe.de/forschung/niobiumoxide/niobiumoxide.html
7. *Tech Topics…The Leading Edge*, Vol. 11, No. 1, KEMET Electronics Corp., Greenville, SC, USA, 2001
8. T. Zednicek, S. Zednicek, Z. Sita, *Technical Information*, AVX Czech Republic s.r.o., AVX Corporation, 2007: http://www.avxcorp.com
9. A. Zylbersztejn, N. F. Mott, *Phys. Rev.* **B11** (1975) 4383
10. M. Gupta, A. J. Freeman, D. E. Ellis, *Phys. Rev.* **B16** (1977) 3338
11. D. Paquet, P. Leroux-Hugon, *Phys. Rev.* **B20** (1980) 5284
12. L. Young, *Anodic Oxide Films*, Academic Press, London, 1961
13. D. A. Vermilyea, in *Advances in Electrochemistry and Electrochemical Engineering*, P. Delahay, Ed., Vol. 3, Interscience, New York, 1963, Ch. 4
14. W. S. Goruk, L. Young, F. G. R. Zobel, in *Modern Aspects of Electrochemistry*, J. O'M. Bockris, Ed., Vol. 4, Plenum Press, New York, 1966, Ch. 3
15. M. J. Dignam, in *Comprehensive Treatise of Electrochemistry*, J. O'M. Bockris, B. E. Conway, E. Yeager, R. E. White, Eds., Vol. 4, Plenum Press, New York, 1981, Ch. 5
16. J. A. Davies, B. Domeij, J. P. S. Pringle, F. Brown, *J. Electrochem. Soc.* **112** (1965) 675
17. A. J. Schrijner, A. Middelhock, *J. Electrochem. Soc.* **111** (1964) 1167
18. D. K. Murti, R. Kelly, *Thin Solid Films* **33** (1976) 149
19. W. Schmickler, J. W. Schultze, in *Modern Aspects of Electrochemistry*, J. O'M. Bockris, B. E. Conway, R. E. White, Eds., Vol. 17, Plenum Press, New York, 1986, Ch. 5
20. S. R. Morrison, *Electrochemistry at Semiconductor and Oxidized Metal Electrodes*, Plenum Press, New York, 1980
21. P. Clechet, J. Martin, R. Oliver, C. Vallony, *C. R. Acad. Sci. Ser.* **C282** (1976) 887
22. A. J. Nozik, *Ann. Rev. Phys. Chem.* **29** (1978) 189
23. T. Hurlen, H. Bentzen, S. Hornkjøl, *Electrochim. Acta* **32** (1987) 1613
24. W. A. Badawy, A. G. Gad-Allah, H. H. Rehan, *J. Appl. Electrochem.* **17** (1987) 559
25. A. G. Gad-Allah, *J. Appl. Electrochem.* **21** (1991) 346
26. A. Robin, *J. Appl. Electrochem.* **32** (2004) 623
27. G. E. Cavigliasso, M. J. Esplandiu, V. A. Macagno, *J. Appl. Electrochem.* **28** (1998) 1213
28. I. Lj. Arsova, A. R. Prusi, Lj. D. Arsov, *J. Solid State Electrochem.* **7** (2003) 217
29. I. Arsova, P. Abduraf, T. Grčev, Lj. Arsov, *J. Serb. Chem. Soc.* **71** (2006) 177.
30. I. Mickova, A. Prusi, T. Grcev, Lj. Arsov, *Croat. Chim. Acta* **79** (2006) 527

31. I. Sieber, H. Hildebrand, A. Friedrich, P. Schmuki, *Electrochem. Comm.* **7** (2005) 97
32. C. Baruffaldi, U. Casellato, S. Cattarin, M. Musiani, B. Tribollet, B. Vercelli, *Electrochim. Acta* **47** (2002) 2989
33. C. Baruffaldi, R. Bertoncello, S. Cattarin, P. Guerriero, M. Musiani, *J. Electroanal. Chem.* **545** (2003) 65
34. S. Cattarin, M. Musiani, *J. Electroanal. Chem.* **517** (2001) 101
35. J. Choi, J. H. Lim, J. Lee, K. J. Kim, *Nanotechnol.* **18** (2007) 055603
36. M. Bojinov, I. Betova, R. Raicheff, *J. Electroanal. Chem*. **411** (1996) 37
37. M. Bojinov, I. Kanazirski, A. Girginov, *Electrochim. Acta* **41** (1996) 2695
38. M. Bojinov, *Electrochim. Acta* **42** (1997) 3489
39. J. R. MacDonald, *Impedance Spectroscopy Emphasizing Solid Materials and Systems*, Wiley, New York, 1987
40. K. Sugimoto, G. Belanger, D. Piron, *J. Electrochem. Soc*. **126** (1979) 535
41. V. Lokshtanov, A. Rotinyan, *Elektrokhimiya* **5** (1969) 873
42. C. D. Alkaine, L. De Souza, F. Nart, *Corr. Sci*. **34** (1993) 109
43. J. van Muylder, N. De Zubov, M. Pourbaix, *Rapport Technique RT-53 of CEBELCOR*, 1957
44. http://www.gamry.com/App_Notes/PDF/jovic.pdf
45. C. H. Hsu, F. Mansfeld, *Corrosion* **57** (2001) 747
46. M. E. Orazem, P. Shukla, M. A. Membrino, *Electrochim. Acta* **47** (2002) 2027
47. V. D. Jović, M. W. Barsoum, B. M. Jović, A. Ganguly, T. El-Raghy, *J. Electrochem. Soc*. **153** (2006) B238
48. N. Ibris, J. C. Mirza Rosca, *J. Electroanal. Chem*. **526** (2002) 53
49. W. Wilhelmsen, *Electrochim. Acta* **33** (1988) 63
50. C. Y. Chao, L. F. Lin, D. D. MacDonald, *J. Electrochem. Soc*. **128** (1981) 1187
51. E. Sikora, D. D. MacDonald, *J. Electrochem. Soc*. **147** (2000) 4087
52. E.-J. Lee, S.-I. Pyun, *J. Appl. Electrochem*. **22** (1992) 156
53. S. Kudelka, J. W. Schultze, *Electrochim. Acta* **42** (1997) 2817
54. W. P. Gomes, D. Vanmaekelbergh, *Electrochim. Acta* **41** (1996) 967
55. J. Sikora, E. Sikora, D. D. MacDonald, *Electrochim. Acta* **45** (2000) 1875
56. E. Sikora, D. D. MacDonald, *Electrochim. Acta* **48** (2002) 69.